Structural basis of antizyme-mediated regulation of polyamine homeostasis

Hsiang-Yi Wu[a], Shin-Fu Chen[a,1], Ju-Yi Hsieh[b,1], Fang Chou[a], Yu-Hsuan Wang[b], Wan-Ting Lin[a,c], Pei-Ying Lee[a,c], Yu-Jen Yu[a], Li-Ying Lin[a,c], Te-Sheng Lin[a,c], Chieh-Liang Lin[a], Guang-Yaw Liu[d,e], Shiou-Ru Tzeng[a,2], Hui-Chih Hung[b,f,2], and Nei-Li Chan[a,c,2]

[a]Institute of Biochemistry and Molecular Biology, College of Medicine, National Taiwan University, Taipei 100, Taiwan; [b]Department of Life Sciences and Institute of Genomics and Bioinformatics, National Chung Hsing University, Taichung 402, Taiwan; [c]Institute of Biochemistry, National Chung Hsing University, Taichung 402, Taiwan; [d]Institute of Microbiology and Immunology, Chung Shan Medical University, Taichung 402, Taiwan; [e]Division of Allergy, Immunology, and Rheumatology, Chung Shan Medical University Hospital, Taichung 402, Taiwan; and [f]Agricultural Biotechnology Center, National Chung Hsing University, Taichung 402, Taiwan

Edited by Wesley I. Sundquist, University of Utah School of Medicine, Salt Lake City, UT, and approved July 21, 2015 (received for review April 28, 2015)

Polyamines are organic polycations essential for cell growth and differentiation; their aberrant accumulation is often associated with diseases, including many types of cancer. To maintain polyamine homeostasis, the catalytic activity and protein abundance of ornithine decarboxylase (ODC), the committed enzyme for polyamine biosynthesis, are reciprocally controlled by the regulatory proteins antizyme isoform 1 (Az_1) and antizyme inhibitor (AzIN). Az_1 suppresses polyamine production by inhibiting the assembly of the functional ODC homodimer and, most uniquely, by targeting ODC for ubiquitin-independent proteolytic destruction by the 26S proteasome. In contrast, AzIN positively regulates polyamine levels by competing with ODC for Az_1 binding. The structural basis of the Az_1-mediated regulation of polyamine homeostasis has remained elusive. Here we report crystal structures of human Az_1 complexed with either ODC or AzIN. Structural analysis revealed that Az_1 sterically blocks ODC homodimerization. Moreover, Az_1 binding triggers ODC degradation by inducing the exposure of a cryptic proteasome-interacting surface of ODC, which illustrates how a substrate protein may be primed upon association with Az_1 for ubiquitin-independent proteasome recognition. Dynamic and functional analyses further indicated that the Az_1-induced binding and degradation of ODC by proteasome can be decoupled, with the intrinsically disordered C-terminal tail fragment of ODC being required only for degradation but not binding. Finally, the AzIN–Az_1 structure suggests how AzIN may effectively compete with ODC for Az_1 to restore polyamine production. Taken together, our findings offer structural insights into the Az-mediated regulation of polyamine homeostasis and proteasomal degradation.

polyamine homeostasis | ornithine decarboxylase | antizyme | antizyme inhibitor | ubiquitin-independent proteolysis

Polyamines are multivalent organic cations that are ubiquitous and essential in eukaryotes (1). With their polycationic characteristics, these compounds are known to modulate the structural and functional properties of nucleic acids and proteins via electrostatic interactions, in turn affecting cell growth and differentiation by influencing the underlying cellular processes (1, 2). Consistent with their crucial regulatory roles, fluctuations in intracellular polyamine levels are rigorously controlled during cell growth and differentiation via fine-tuning the balance between the biosynthesis, degradation, and uptake of polyamines. Aberrant accumulation of polyamines is associated with pathological consequences, including many types of cancer (3–5).

Regulation of polyamine homeostasis is achieved mainly by adjusting the catalytic activity and protein abundance of ornithine decarboxylase (ODC), a homodimeric and pyridoxal 5′-phosphate-dependent enzyme that catalyzes the committed and rate-limiting step in polyamine biosynthesis, through the actions of the regulatory proteins antizyme isoform 1 (Az_1) and antizyme inhibitor (AzIN) (3, 6). Elevation of cellular polyamine levels induces the translation of the full-length Az_1, an intracellular ODC inhibitory protein, by stimulating the bypassing of an in-frame stop codon on Az_1 mRNA (7, 8) and by relieving the translational repression effect mediated through the N-terminal fragment of Az_1 (9). The formation of the ODC–Az_1 heterodimer blocks the assembly of the functional ODC homodimer to inhibit polyamine production (10). Moreover, Az_1 can completely shut down the polyamine biosynthetic pathway by targeting ODC for proteolytic destruction via the 26S proteasome (11). Although ubiquitylation is a predominant pathway that channels proteins for proteasomal degradation, Az-induced ODC degradation is unique in its ubiquitin-independent nature. The identification of antizyme isoform 2 (Az_2) and antizyme isoform 3 (Az_3) (12, 13), the tissue and development-specific Az isoforms, further underscores the physiological significance of keeping the cellular polyamine concentrations under tight control. Unlike Az_1, however, Az_2 and Az_3 simply inhibit the catalytic activity of ODC without promoting its degradation, which allows a protein synthesis-independent restoration of ODC activity (6).

Replenishment of the intracellular polyamine pool requires the expression of AzIN, an enzymatically inactive ODC homolog,

Significance

Polyamines are small organic compounds that carry multiple positive charges at physiological pH. With a high capacity to interact with the acidic surface patches of proteins and nucleic acids, polyamines may regulate a variety of cellular processes, and the fluctuations in the intracellular polyamine levels are rigorously controlled during cell growth and differentiation through the interplay between the enzyme ornithine decarboxylase (ODC) and two regulatory proteins: antizyme (Az) and antizyme inhibitor (AzIN). ODC initiates the polyamine biosynthetic pathway, whereas Az decreases polyamine concentrations by both inhibiting ODC activity and channeling ODC for proteolytic degradation. AzIN neutralizes Az function to restore polyamine levels. Here we provide the long-sought structural information and previously unidentified functional insights into this delicate regulatory circuit.

Author contributions: H.-Y.W., S.-F.C., S.-R.T., H.-C.H., and N.-L.C. designed research; H.-Y.W., S.-F.C., J.-Y.H., F.C., Y.-H.W., W.-T.L., P.-Y.L., Y.-J.Y., C.-L.L., and S.-R.T. performed research; H.-Y.W., S.-F.C., J.-Y.H., F.C., Y.-H.W., W.-T.L., P.-Y.L., Y.-J.Y., L.-Y.L., T.-S.L., G.-Y.L., S.-R.T., H.-C.H., and N.-L.C. analyzed data; and H.-Y.W., S.-F.C., S.-R.T., H.-C.H., and N.-L.C. wrote the paper.

The authors declare no conflict of interest.

This article is a PNAS Direct Submission.

Data deposition: The atomic coordinates and structure factors have been deposited in the Protein Data Bank, www.pdb.org (PDB ID codes 4ZGY and 4ZGZ).

[1]S.-F.C. and J.-Y.H. contributed equally to this work.

[2]To whom correspondence may be addressed. Email: nlchan@ntu.edu.tw, srtzeng@ntu.edu.tw, or hchung@dragon.nchu.edu.tw.

This article contains supporting information online at www.pnas.org/lookup/suppl/doi:10.1073/pnas.1508187112/-/DCSupplemental.

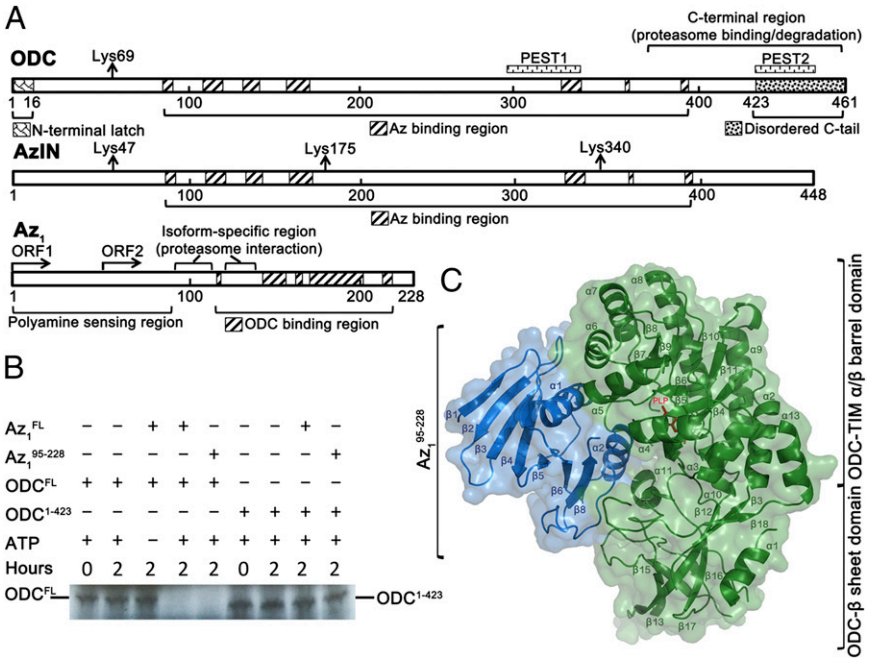

Fig. 1. The ODC–$Az_1^{95–228}$ structure represents the first view of a substrate protein primed for ubiquitylation-independent proteasomal degradation. (*A*) Linear organization of functional domains and motifs of human ODC (*Top*), AzIN (*Middle*), and Az_1 (*Bottom*). For ODC, the N-terminal latch and Az_1 binding regions are defined in this study. The C-terminal region that functions as a putative "degradation signal," the pyridoxal 5′-phosphate-binding residue (K69), the PEST sequences, and the intrinsically disordered C-tail of ODC were defined previously (3, 18, 19). For AzIN, the Az_1 binding regions (defined in this work) and the reported ubiquitylation sites are indicated (28). For Az_1, the *N*- and C-terminal domains and the ODC/AzIN-binding regions (defined in this work) are indicated. ORF1 of Az_1 mRNA is normally translated, whereas continuous translation into ORF2 to form the full-length Az_1 requires a polyamine-stimulated +1 frame shift at the ORF1/ORF2 boundary (7, 8). (*B*) $Az_1^{95–228}$ efficiently promotes the proteasomal degradation of ODC, whereas the C-tail–truncated mutant ($ODC^{1–423}$) is proteolysis resistant in the reticulocyte lysate-based in vitro degradation assay. (*C*) Crystal structure of the human ODC–$Az_1^{95–228}$ complex in ribbon representation. ODC and $Az_1^{95–228}$ are colored green and blue, respectively; pyridoxal 5′-phosphate is shown in red stick.

which effectively restores ODC activity by competing with ODC for Az_1 binding (6, 14). Together, ODC, AzIN, and the various Az isoforms form a delicate regulatory circuit to coordinate polyamine biosynthesis, in which ODC and AzIN serve as positive regulators and are considered oncogenic because they promote cell growth and transformation (15). In contrast, Az isoforms are tumor suppressors whose ectopic expression inhibits cell proliferation and tumorigenesis (16).

Although the Az_1-mediated regulation of polyamine homeostasis bears high biological and medical significance, our understanding of the underlying molecular basis has remained incomplete due to the lack of structural information about the ODC–Az_1 and AzIN–Az_1 complexes. This study fills in this gap by providing for the first time, to our knowledge, the crystal structures of the two complexes. Moreover, the accompanying solution NMR and biochemical analysis revealed previously unidentified insights into the Az_1-mediated recognition and degradation of ODC by the 26S proteasome.

Results and Discussion

Az_1 Inhibits ODC Activity by Physically Blocking Assembly of the Functional ODC Homodimer. To understand how ODC is enzymatically inactivated and targeted for proteasomal degradation upon Az_1 binding, we determined the crystal structure of human ODC in complex with an N-terminal truncated Az_1 ($Az_1^{95–228}$; covering residues 95∼228) (Fig. 1*A* and Table S1). Because $Az_1^{95–228}$ exhibits wild type-like ODC binding affinity and inhibition activity (17) and efficiently promotes ODC degradation in a reticulocyte lysate-based degradation system (Fig. 1*B*), the ODC–$Az_1^{95–228}$ structure represents the first observation, to our knowledge, of a substrate protein that is primed to be recognized by the 26S proteasome without the need for ubiquitylation (Fig. 1*C*). The functional relevance of the observed heterodimerization interface was illustrated by the finding that the ODC–$Az_1^{95–228}$ dimer may be destabilized by mutations at contact residues, albeit to different degrees (Table 1 and Fig. S1). Importantly, the Az_1-contacting surface overlaps substantially with the homodimerization interface of ODC (Fig. S2), providing a rationalization for how the binding of Az_1 to a transiently formed ODC monomer would effectively repress polyamine biosynthesis by inhibiting the assembly of the catalytically active ODC homodimer.

The ODC homodimer (18) and the ODC–$Az_1^{95–228}$ heterodimer bury ∼5,400 and ∼3,200 Å^2 of solvent-accessible surface area (ASA), respectively. Given that these two interfaces exhibit similar ratios of nonpolar to polar residues (Fig. S2), their relative stability is expected to correlate positively with the corresponding interface area. Consequently, the formation of two ODC–Az_1 heterodimers, which produces a combined ∼6,400 Å^2 of buried ASA, upon the disruption of one ODC homodimer would appear to be energetically favorable with a net gain of an additional ∼1,000 Å^2 of buried ASA, and a dose-dependent suppression of ODC activity by Az_1 can be observed even when Az_1 is present at substoichiometry levels (17). Therefore, feedback inhibition of polyamine biosynthesis is immediately engaged upon the production of Az_1.

Az_1 Binding Primes ODC for Ubiquitin-Independent Proteasome Recognition. When present individually, neither Az_1 nor ODC shows appreciable binding to the proteasome, whereas the ODC–Az_1 complex is efficiently recognized by the proteasome for degradation (Fig. 1*B*), indicating that a proteasome-interacting surface is formed upon heterodimerization (11). By analyzing the competency of various mutant and chimeric ODCs as substrates for degradation, an essential element for directing polyamine-induced ODC degradation has been mapped to the C-terminal

Table 1. Dissociation constants of human ODC–Az complexes

Protein variant	$K_{d,ODC–Az}$, μM
ODC–Az	0.7 ± 0.01
[ODC_S118A]–Az	5.3 ± 0.04
[ODC_D134A]–Az	8.1 ± 0.06
[ODC_S135A]–Az	2.4 ± 0.02
[ODC_Y331A]–Az	3.2 ± 0.03
[ODC_D361A]–Az	13.9 ± 0.23
[ODC_F397A]–Az	1.9 ± 0.02
[ODC_S118A/D134A]–Az	8.2 ± 0.07
ODC–[Az_K153A/E164A]	5.3 ± 0.04

The dissociation constants (K_d) of ODC–Az were derived from global fitting of the sedimentation velocity data shown in Fig. S1 to the model of A+B↔AB heteroassociation using the SEDPHAT program (30).

region of ODC (residues 376~461; Fig. 1*A*) (19). Antibodies raised against this region were found to react significantly stronger in the presence of Az_1; the enhanced presentation of epitopes suggests the occurrence of an Az_1-induced conformational change in ODC, which likely evokes the exposure of a proteasome-interacting element. Structural comparison of ODC–Az_1^{95-228} to the ODC homodimer revealed a marked difference in the solvent accessibility of the middle portion of this region (residues 395~421) (Fig. 2*A*). In the context of the ODC homodimer, this fragment is partially buried by the neighboring ODC subunit and by packing against the protomer's own N terminus (residues 7~16) (18). Intriguingly, in ODC–Az_1^{95-228}, the fragment becomes fully exposed and thus appears to be suitable for mediating proteasome association due to the disruption of the homodimer interface and an Az_1-induced structural transition of the ODC N terminus, which becomes disordered and invisible in the electron density map upon Az_1 binding (Fig. 2*B*). MALDI-TOF mass spectrometry and N-terminal sequencing analysis using an ODC protein sample retrieved from dissolved ODC–Az_1^{95-228} crystals both show the intactness of the ODC N terminus (Fig. S3), providing convincing evidence that the exposure of this presumably proteasome-interacting surface of ODC is caused by an Az_1-induced order-to-disorder transition of the ODC N-terminal segment (Fig. 2), rather than by an experimental artifact that resulted from non-specific proteolysis during sample preparation and crystallization. This N-terminal segment of ODC (residues 1~16) is hereafter referred to as the *N*-latch (Fig. S4 and Fig. 1*A*), whose conformation is locked in the ODC homodimer by binding across the barrel and sheet domains to mask a prospective proteasome-interacting surface. Az_1 binding causes both significant repositioning of the two domains of ODC and rearrangement of the interface contacts (Fig. 2 *B* and *C*), which disrupt their interactions with the *N*-latch and lead to its displacement.

A comparison between the crystal structure of ODC-bound human Az_1^{95-228} to the solution structure of an N-terminal truncated rat Az_1 determined by NMR spectroscopy (20) revealed differences in the relative orientations of several loop regions (Fig. S5). The changes observed in the β3–β4, β5–α1, β6–α2, and α2–β8 loops appear functionally relevant because these regions are involved in the heterodimerization with ODC, indicating that Az_1 would undergo conformational adjustments upon ODC binding. Unlike ODC, whose proteasome-interacting surface is

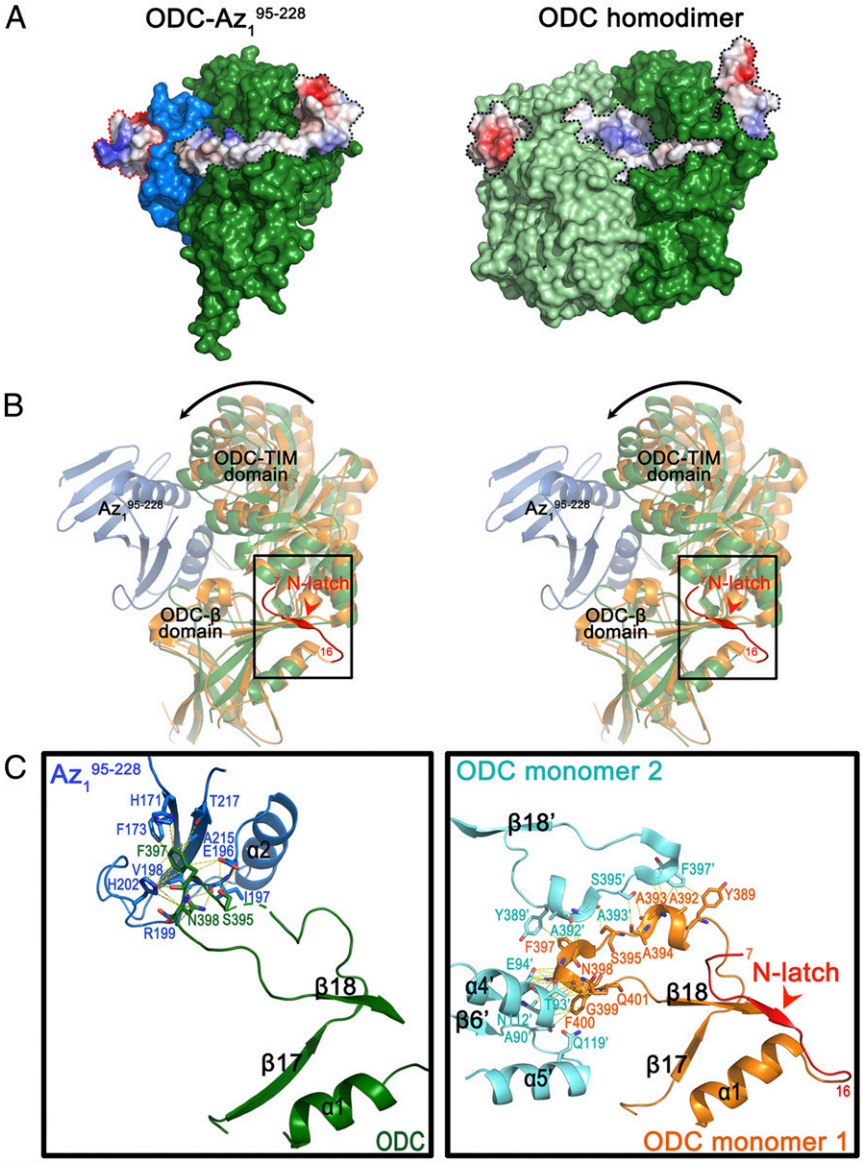

Fig. 2. ODC is primed for proteasome recognition by associating with Az_1 and by exhibiting Az_1-induced conformational changes. (*A*) ODC–Az_1^{95-228} (*Left*) and the ODC homodimer (*Right*) exhibit distinct surface features, consistent with the difference in their proteasome-targeting potentials. The surfaces of ODC and Az_1 are colored green (or pale green for the second ODC protomer) and blue, respectively, and the predicted proteasome-interacting surfaces of ODC and Az_1 (enclosed by black and red dashed lines, respectively) are highlighted according to the electrostatic potential of the constituent atoms (blue, positive; red, negative; white, neutral). Az_1 binding induces structural changes in ODC that lead to the formation of an extensive surface composed of the proteasome-interacting elements of both proteins. (*B*) Stereoview of a superposition of the human ODC monomer structure [Protein Data Bank (PDB) ID code 1D7K (18); orange] and the Az_1-bound ODC structure (this study; green) reveals Az_1-induced repositioning of the two ODC domains and the order-to-disorder transition of the *N*-latch fragment (red arrowhead, enclosed by the black box). The β domains of ODC monomers were superimposed to illustrate the clamp-like domain movement. (*C*) In the ODC homodimer (*Right*), the loop region spanning residues 390–405 (orange), which is involved in dimerization and may play a role in proteasome recognition, forms two short helical turns and packs against the *N*-latch fragment. In ODC–Az_1^{95-228} (*Left*), this loop (green) mediates a different set of interactions and adopts an alternative conformation. Labels belonging to ODC monomer 2 are flagged by a prime.

uncovered only upon its association with Az_1, the surface region of Az_1 (residues 95–145) that has been implicated in proteasome binding (21) shows no ODC-induced change in accessibility. It is noteworthy that the proposed proteasome-interacting elements of both ODC and Az_1 are placed in close proximity in ODC–$Az_1^{95–228}$ (Fig. 2*A*); together an extensive surface composed of multiple loop regions is formed to mediate efficient binding of the heterodimer by proteasome.

Association of the ODC–Az_1 Complex with the 26S Proteasome and the Subsequent Degradation of the Bound ODC Can Be Decoupled. The C-tail fragment of ODC (residues 424–461; Fig. 1*A*) is known for its pivotal role in mediating the proteasomal degradation of ODC (19, 22). However, whether the ODC C-tail is involved in the recognition and binding of ODC–Az_1 by the proteasome or whether it is required for initiating subsequent proteolytic events has remained undefined. X-ray crystallography failed to provide structural information about the ODC C-tail because this region is disordered in the structures of both the ODC–$Az_1^{95–228}$ heterodimer and the ODC homodimers (18). Given the sensitivity of chemical shifts to the environmental changes, we assessed whether the structural and dynamic properties of the ODC C-tail are altered upon Az_1 binding using NMR spectroscopy. The one-dimensional ^{1}H-NMR spectrum of the 102 kDa ODC homodimer revealed narrowly dispersed resonances with all amide proton chemical shifts confined to ~7.8–8.7 ppm, indicating that portions of the homodimer exhibit inherent conformational flexibility. A series of 2D ^{1}H–^{15}N heteronuclear single-quantum coherence (HSQC) spectra were acquired for the full-length and the C-tail–truncated ODC ($ODC^{1–423}$) in both the homodimeric and ODC–$Az_1^{95–228}$-bound heterodimeric forms (Fig. 3*A*). Comparing the spectra of the full-length and truncated homodimers showed that the ODC C-tail is indeed unstructured, being highly flexible and solvent exposed, which gives rise to well-resolved NMR peaks. Moreover, the signals that correspond to the ODC C-tail remained unchanged in the presence of $Az_1^{95–228}$ (Fig. 3*B*), suggesting that heterodimerization most likely has no effect on the properties of this region.

We further probed the backbone dynamics and quantified the flexibility of ODC in different states using heteronuclear ^{1}H–^{15}N nuclear Overhauser effect (NOE) experiments, such that the motion of individual *N*–H bond vectors with sign and magnitude can be obtained to reflect the mobility relative to the overall molecular tumbling rate of the protein and also relative to the internal dynamics. The average values of ^{1}H–^{15}N NOE for the ODC C-tail in the homodimeric and heterodimeric states are –0.76 and –0.80, respectively, and the relatively large negative NOE values are indicative of the significant motions of the bond vectors that occur on a fast timescale and arise from an unstructured region. Therefore, the relatively similar NOE values revealed that the high degree of flexibility of the ODC C-tail is retained despite the switching of binding partners. Taken together, the NMR data show that the ODC C-tail exhibits no Az_1-induced structural change.

Because the structural and dynamic properties of the ODC C-tail are not affected by Az_1 binding, we speculated that the exposure of ODC residues 395–421 that resulted from the Az_1-induced *N*-latch movement may be sufficient for targeting the ODC–Az_1 complex to the proteasome. To test this hypothesis, $Az_1^{95–228}$ was mixed with either full-length ODC or the C-tail truncation mutant $ODC^{1–423}$, and the reconstituted heterodimers were used to pull down proteasomes from cell lysates treated with the proteasome inhibitor MG132 (Fig. 3*C*). The results clearly show that ODC–$Az_1^{95–228}$ and $ODC^{1–423}$–$Az_1^{95–228}$ interacted equally efficiently with proteasomes, as judged by the similar amounts of the proteasome lid subunit S5a being pulled down by the two heterodimers, and hence the ODC C-tail is dispensable for the Az_1-directed association of ODC with the proteasome. Although not required for proteasome binding, the ODC C-tail is absolutely essential for mediating degradation

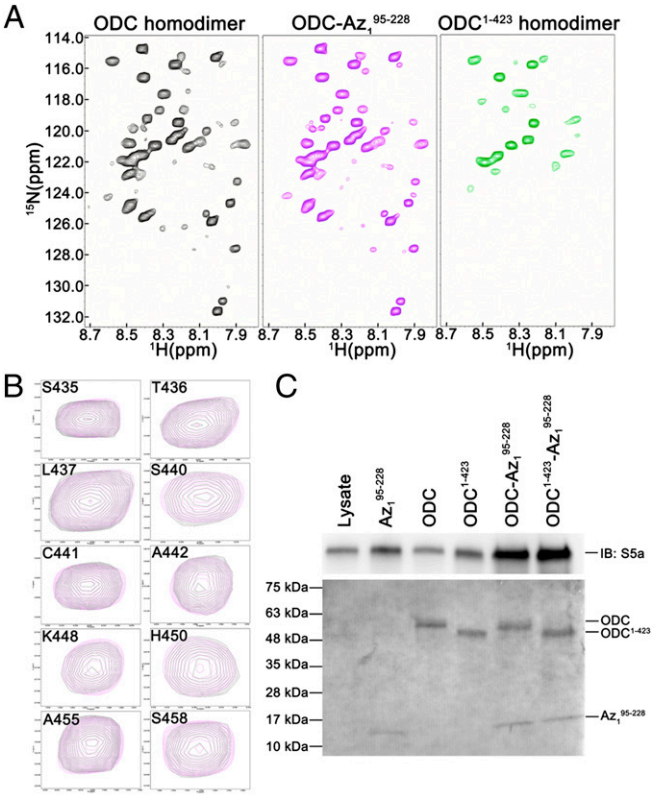

Fig. 3. Structural and dynamic properties of the intrinsically disordered ODC C-tail are not affected by Az_1 binding. (*A*) ^{1}H–^{15}N HSQC spectra datasets of uniformly ^{15}*N*-labeled ODC in the absence (*Left*, black) or presence of equimolar amounts of unlabeled $Az_1^{95–228}$ (*Middle*, magenta) show no chemical-shift perturbations at the C-tail upon heterodimer formation. The spectrum of the ODC C-tail truncation mutant ($ODC^{1–423}$) is shown in the *Right* panel (green). (*B*) Overlaid ^{1}H–^{15}N HSQC spectra of ODC in homodimeric (black) and $Az_1^{95–228}$-bound heterodimeric (magenta) states. The chemical shifts of the ODC C-tail residues are essentially identical in the two states, demonstrating that the structural and dynamic properties of this region are not affected by Az_1 binding. (*C*) A coimmunoprecipitation assay shows that ODC–$Az_1^{95–228}$ and $ODC^{1–423}$–$Az_1^{95–228}$ interact equally efficiently with the proteasome (as indicated by the level of the pulled down proteasome subunit S5a), suggesting that the ODC C-tail is dispensable for the Az_1-mediated proteasome targeting of ODC. IB, immunoblotted with anti-S5a antibody. The *Upper* portion shows the result of immunoblotting with anti-S5A antibody (IB: S5a); the lower portion shows the image of electroblotted membrane stained with Ponceau S to validate that equal amounts of Az, ODC, or ODC-Az complex were used for the coimmunoprecipitation assay.

because $ODC^{1–423}$ remained stable in a reticulocyte lysate-based degradation assay in the presence of Az_1, whereas the full-length ODC was readily degraded (Fig. 1*B*, comparing lanes 4 and 8). Recent studies have elucidated the significance of having a disordered region present on a substrate protein for prompting proteasomal degradation (23, 24). Our findings support the role of the ODC C-tail as the disordered element required for triggering degradation after the ODC–Az_1 complex is captured by the proteasome.

Functional Extrapolation of Az_2 and Az_3. The ODC–Az_1 structure also allows the extrapolation of the function of other Az isoforms. Sequence analysis revealed that the majority of the residues involved in ODC binding are conserved across all Az members (Fig. S6), indicating that Az_2 and Az_3 would also target the Az_1-contacting surface of ODC and inhibit its enzymatic function via the formation of heterodimers with a similar architecture. However, except for the similarity in their ODC binding areas,

the surface features of Az_2 and Az_3 differ from those of Az_1. The modulations of the proteasome-interacting surface explain why the alternative heterodimers cannot be recognized by the proteasome, consistent with the roles of Az_2 and Az_3 as simple catalytic inhibitors of ODC (21, 25).

Structural Analysis of the AzIN–Az_1 Complex. The Az_1-mediated down-regulation of polyamine levels can be effectively antagonized by AzIN, an enzymatically inactive ODC homolog, whose higher affinity for Az_1 suppresses the formation of the ODC–Az_1 complex and thus restores ODC activity (6). To understand how AzIN may interact more strongly with Az_1, we have produced crystals of AzIN in complex with an Az_1 C-terminal fragment ($Az_1^{110–228}$; covering residues 110–228) that diffract to 5.8 Å resolution (Table S1). Initial phases were obtained by molecular replacement using a polyalanine search model derived from the mouse AzIN structure (26), which yielded an unbiased electron density suitable for the placement of $Az_1^{110–228}$ (Fig. 4*A*). Modeling of the side chains into both proteins was accomplished by referencing to the corresponding high-resolution structures, and the structure of the AzIN–$Az_1^{110–228}$ complex was determined with reasonable statistics and stereochemistry (Fig. 4*B* and Table S1). Despite their low-resolution nature, the structural features of AzIN and $Az_1^{110–228}$ closely resemble the high-resolution structures of AzIN (26) and $Az_1^{95–228}$ with the rmsds from the superposition being 1.2 and 0.7 Å, respectively, over all equivalent main-chain atom pairs (Fig. S7). The overall architecture of AzIN–$Az_1^{110–228}$ approximates that of ODC–$Az_1^{95–228}$, with the same surface of Az_1 being recognized by the barrel and sheet domains (Figs. 1*C* and 4*B* and Figs. S2 and S8). The majority of the residues involved in Az_1 binding are either identical or conserved between ODC and AzIN, except that N327 and Y331 of ODC are replaced by A325 and S329 in AzIN (Fig. S8). Notably, these two amino acid substitutions are conserved essentially across all vertebrate AzINs; thus, we speculate that the resulting changes in the shape and polarity of the Az_1-interacting surface may partly contribute to the stronger association between AzIN and Az_1. Moreover, although ODC undergoes domain repositioning and *N*-latch movement upon Az_1 binding (Fig. 2*B*), the structures of apo and Az_1-bound AzIN exhibit greater similarity (Fig. 4*C*). It appears that the two domains of AzIN are already in position to interact with Az_1. Thus, compared with the assembly of ODC–Az_1, the formation of the AzIN–Az_1 complex may be energetically more favored with a milder loss of conformational entropy.

The AzIN–$Az_1^{110–228}$ structure also illustrates how AzIN–Az_1 interactions may be modulated to produce adverse health effects. An S367-to-glycine mutation that resulted from an adenosine deaminase-mediated editing of AzIN mRNA was shown to drive tumorigenesis by raising the cellular polyamine levels via an increase in the association between AzIN and Az_1 (27). Although not directly involved in Az_1 binding, this substitution was suggested to induce structural change of a conformational switch region of AzIN that lies adjacent to the heterodimerization interface, thus affecting the association between Az_1 and the tumorigenic form of AzIN.

Intriguingly, rather than targeting AzIN for proteasomal degradation, Az_1 binding instead prolongs the half-life of AzIN, possibly by preventing its polyubiquitylation. In the AzIN–$Az_1^{110–228}$ structure, the AzIN segment corresponding to the *N*-latch of ODC does not undergo an Az_1-induced structural transition, and an AzIN-specific interaction between its *N* and C segments also remains intact. Together, these two effects render the AzIN surface sufficiently different from ODC (Fig. S9), which explains why the AzIN–Az_1 complex cannot be recognized by the proteasome. Mapping the three prospective ubiquitylation sites identified by a proteome-wide mass spectrometric analysis (28) onto the AzIN–$Az_1^{110–228}$ structure revealed that none of the target lysine residues are shielded by the bound Az_1, suggesting that Az_1 binding likely weakens or prohibits the interaction between AzIN and E3 ubiquitin ligases.

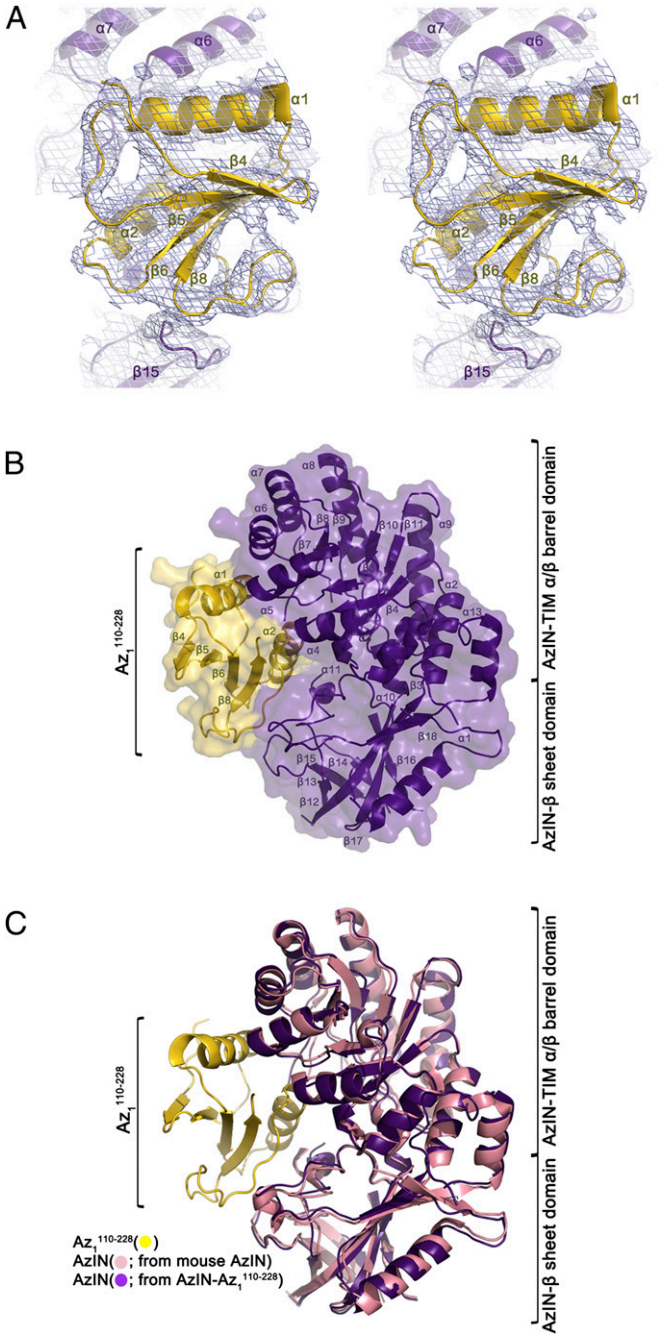

Fig. 4. Structural analysis of the human AzIN–$Az_1^{110–228}$ heterodimer. (*A*) A section from a 5.8 Å resolution electron density map of the AzIN–$Az_1^{110–228}$ complex. Molecular replacement phasing using a polyalanine search model derived from the mouse AzIN structure (26) produced electron density (blue mesh, 1.0-σ cutoff) that is not biased toward $Az_1^{110–228}$. Ribbon representations of the AzIN and $Az_1^{110–228}$ are in purple and yellow, respectively. Note that the refined $Az_1^{110–228}$ model fits nicely in the density. (*B*) Ribbon representation of the AzIN (purple) in complex with $Az_1^{110–228}$ (yellow) determined at a 5.8 Å resolution. (*C*) Structural superposition of the mouse AzIN monomer [PDB ID code 3BTN (26); pink] and the Az_1-bound human AzIN (purple) reveals the lack of significant repositioning of the two AzIN domains upon Az_1 binding.

Conclusion

In summary, our structural analysis demonstrates that Az_1 shuts down polyamine biosynthesis by physically blocking the formation of the catalytically active ODC homodimer and by targeting ODC for ubiquitylation-independent proteolysis via exposing a

cryptic proteasome-interacting surface. Dynamic and functional analyses further reveal that the association of the ODC–Az_1 complex with the proteasome and the subsequent degradation of the bound ODC can be decoupled, with the intrinsically disordered ODC C-terminal tail being dispensable for binding but required for degradation. Additionally, we suggest a structural basis by which AzIN competes with ODC for Az_1 to restore polyamine biosynthesis. In addition to its interactions with ODC and AzIN, Az_1 also binds and inhibits a polyamine-specific transporter on the plasma membrane and may target various crucial regulatory proteins, including cyclin D1, Aurora-A kinase, Smad1, DeltaNp73, and Mps1, for proteasomal degradation (1). It remains to be determined how these structurally distinct proteins interact with Az_1 and how the resulting complexes are processed by the 26S proteasome.

Materials and Methods

The ODC–$Az_1^{95–228}$ and AzIN–$Az_1^{110–228}$ complexes were produced in *Escherichia coli*. The ODC–Az_1^{95-228} crystals formed in 100 mM magnesium acetate, 50 mM MES (pH 5.6), and 20% (vol/vol) 2-methyl-2, 4-pentanediol. The AzIN–$Az_1^{110–228}$ crystals formed in 0.1 M *N*-(2-acetamido) iminodiacetic acid (pH 6.5) and 1.0 M ammonium sulfate. The structures were solved and refined using Python-based Hierarchical ENvironment for Integrated Xtallography (PHENIX) (29). Complete methods for sample preparation, protein crystallization, structure determination, NMR spectroscopy, in vitro degradation reaction, coimmunoprecipitation, site-directed mutagenesis, and analytical ultracentrifugation are described in *SI Materials and Methods*.

ACKNOWLEDGMENTS. We thank Y.-C. Li and L.-Y. Chen for help with MALDI MS analysis and preparation of cell lysates and members of our laboratories for helpful discussion. We also thank S.-J. Huang (Instrumentation Center, National Taiwan University) for help in acquiring NMR data with Bruker AVIII 800 MHz NMR spectrometer. We are grateful to the staffs of Technology Commons in College of Life Science and Center for Systems Biology, National Taiwan University. Portions of this research were carried out at beamlines 15A1 and 13B1 of the National Synchrotron Radiation Research Center (Taiwan) and beamline SP12B2 of the SPring-8 (Japan).This work was supported by Ministry of Science and Technology Grants NSC101-2911-I-002-303, 103-2113-M-002-010-MY3, and 104-2911-I-002-302; National Research Program for Biopharmaceuticals Grant NSC101-2325-B-002-049; National Taiwan University Grants 104R7614-3 and 104R7560-4; and the Ministry of Education, Taiwan, under the Aiming for the Top University plan to N.-L.C. (National Chung Hsing University), and National Taiwan University Grants 104R7881 and NSC102-2113-M-002-001-MY2 to (S.-R.T.).

1. Suzuki H, Kusano T (2015) *Polyamines: A Universal Molecular Nexus for Growth, Survival, and Specialized Metabolism* (Springer, Japan).
2. Coffino P (2001) Regulation of cellular polyamines by antizyme. *Nat Rev Mol Cell Biol* 2(3):188–194.
3. Pegg AE (2006) Regulation of ornithine decarboxylase. *J Biol Chem* 281(21):14529–14532.
4. Casero RA, Jr, Marton LJ (2007) Targeting polyamine metabolism and function in cancer and other hyperproliferative diseases. *Nat Rev Drug Discov* 6(5):373–390.
5. Olsen RR, Zetter BR (2011) Evidence of a role for antizyme and antizyme inhibitor as regulators of human cancer. *Mol Cancer Res* 9(10):1285–1293.
6. Kahana C (2009) Antizyme and antizyme inhibitor, a regulatory tango. *Cell Mol Life Sci* 66(15):2479–2488.
7. Matsufuji S, et al. (1995) Autoregulatory frameshifting in decoding mammalian ornithine decarboxylase antizyme. *Cell* 80(1):51–60.
8. Rom E, Kahana C (1994) Polyamines regulate the expression of ornithine decarboxylase antizyme in vitro by inducing ribosomal frame-shifting. *Proc Natl Acad Sci USA* 91(9): 3959–3963.
9. Kurian L, Palanimurugan R, Gödderz D, Dohmen RJ (2011) Polyamine sensing by nascent ornithine decarboxylase antizyme stimulates decoding of its mRNA. *Nature* 477(7365):490–494.
10. Fujita K, Matsufuji S, Murakami Y, Hayashi S (1984) Antizyme to ornithine decarboxylase is present in the liver of starved rats. *Biochem J* 218(2):557–562.
11. Murakami Y, et al. (1992) Ornithine decarboxylase is degraded by the 26S proteasome without ubiquitination. *Nature* 360(6404):597–599.
12. Ivanov IP, Gesteland RF, Atkins JF (1998) A second mammalian antizyme: Conservation of programmed ribosomal frameshifting. *Genomics* 52(2):119–129.
13. Ivanov IP, Rohrwasser A, Terreros DA, Gesteland RF, Atkins JF (2000) Discovery of a spermatogenesis stage-specific ornithine decarboxylase antizyme: antizyme 3. *Proc Natl Acad Sci USA* 97(9):4808–4813.
14. Murakami Y, Ichiba T, Matsufuji S, Hayashi S (1996) Cloning of antizyme inhibitor, a highly homologous protein to ornithine decarboxylase. *J Biol Chem* 271(7): 3340–3342.
15. Auvinen M, Paasinen A, Andersson LC, Hölttä E (1992) Ornithine decarboxylase activity is critical for cell transformation. *Nature* 360(6402):355–358.
16. Iwata S, et al. (1999) Anti-tumor activity of antizyme which targets the ornithine decarboxylase (ODC) required for cell growth and transformation. *Oncogene* 18(1): 165–172.
17. Hsieh JY, Yang JY, Lin CL, Liu GY, Hung HC (2011) Minimal antizyme peptide fully functioning in the binding and inhibition of ornithine decarboxylase and antizyme inhibitor. *PLoS One* 6(9):e24366.
18. Almrud JJ, et al. (2000) Crystal structure of human ornithine decarboxylase at 2.1 A resolution: Structural insights to antizyme binding. *J Mol Biol* 295(1):7–16.
19. Li X, Coffino P (1993) Degradation of ornithine decarboxylase: Exposure of the C-terminal target by a polyamine-inducible inhibitory protein. *Mol Cell Biol* 13(4): 2377–2383.
20. Hoffman DW, Carroll D, Martinez N, Hackert ML (2005) Solution structure of a conserved domain of antizyme: A protein regulator of polyamines. *Biochemistry* 44(35): 11777–11785.
21. Chen H, MacDonald A, Coffino P (2002) Structural elements of antizymes 1 and 2 are required for proteasomal degradation of ornithine decarboxylase. *J Biol Chem* 277(48):45957–45961.
22. Zhang M, Pickart CM, Coffino P (2003) Determinants of proteasome recognition of ornithine decarboxylase, a ubiquitin-independent substrate. *EMBO J* 22(7): 1488–1496.
23. Prakash S, Tian L, Ratliff KS, Lehotzky RE, Matouschek A (2004) An unstructured initiation site is required for efficient proteasome-mediated degradation. *Nat Struct Mol Biol* 11(9):830–837.
24. Berko D, et al. (2012) The direction of protein entry into the proteasome determines the variety of products and depends on the force needed to unfold its two termini. *Mol Cell* 48(4):601–611.
25. Snapir Z, Keren-Paz A, Bercovich Z, Kahana C (2009) Antizyme 3 inhibits polyamine uptake and ornithine decarboxylase (ODC) activity, but does not stimulate ODC degradation. *Biochem J* 419(1):99–103.
26. Albeck S, et al. (2008) Crystallographic and biochemical studies revealing the structural basis for antizyme inhibitor function. *Protein Sci* 17(5):793–802.
27. Chen L, et al. (2013) Recoding RNA editing of AZIN1 predisposes to hepatocellular carcinoma. *Nat Med* 19(2):209–216.
28. Kim W, et al. (2011) Systematic and quantitative assessment of the ubiquitin-modified proteome. *Mol Cell* 44(2):325–340.
29. Adams PD, et al. (2010) PHENIX: A comprehensive Python-based system for macromolecular structure solution. *Acta Crystallogr D Biol Crystallogr* 66(Pt 2):213–221.
30. Dam J, Schuck P (2005) Sedimentation velocity analysis of heterogeneous protein-protein interactions: Sedimentation coefficient distributions c(s) and asymptotic boundary profiles from Gilbert-Jenkins theory. *Biophys J* 89(1):651–666.
31. Minor W, Cymborowski M, Otwinowski Z, Chruszcz M (2006) HKL-3000: The integration of data reduction and structure solution–From diffraction images to an initial model in minutes. *Acta Crystallogr D Biol Crystallogr* 62(Pt 8):859–866.
32. Emsley P, Cowtan K (2004) Coot: Model-building tools for molecular graphics. *Acta Crystallogr D Biol Crystallogr* 60(Pt 12 Pt 1):2126–2132.
33. Kahana C (2011) Identification, assay, and functional analysis of the antizyme inhibitor family. *Methods Mol Biol* 720:269–278.
34. Schuck P, Perugini MA, Gonzales NR, Howlett GJ, Schubert D (2002) Size-distribution analysis of proteins by analytical ultracentrifugation: Strategies and application to model systems. *Biophys J* 82(2):1096–1111.
35. Laue TM, Shah BD, Ridgeway TM, Pelletier SL (1992) *Analytical Ultracentrifugation in Biochemistry and Polymer Science* (The Royal Society of Chemistry, Cambridge, UK).